GEOMETRIC INFERENCE-BASED OBSERVABILITY ANALYSIS DIGEST OF INS ERROR MODEL WITH GPS/MAGNETOMETER/CAMERA AIDING

Ronan Arraes Jardim Chagas[1]
ronan.jardim@gmail.com, Tel: +55.12.97508686
Instituto Tecnológico de Aeronáutica, São José dos Campos (Brazil)

Jacques Waldmann[2]
jacques@ita.br, Tel: +55.12.39475993, Fax:+55.12.39476930
Instituto Tecnológico de Aeronáutica, São José dos Campos (Brazil)

Abstract

Key words: observability analysis, inertial navigation systems, Kalman filter.

A stand-alone inertial navigation system (INS) yields time-diverging solutions due to errors in the inertial sensors, which can inhibit long term navigation. To circumvent this issue, a set of non-inertial sensors is used to limit these errors. The fusion between additional data and INS solution is often done by means of an extended Kalman filter using a state-error model. However, the Kalman filter estimates can only be used if the system is fully observable. This paper has analyzed conditions to achieve full observability under different scenarios using as non-inertial sensors GPS, magnetometer, and camera. Some results in the literature have been revisited, and novel results have been achieved regarding the observability analysis when the INS is aided by a magnetometer. The observability for all scenarios has been verified when the system dynamics is piece-wise constant, and the analysis has been carried out using concepts of linear algebra to provide results that are geometrically meaningful. The novel results obtained in the case of magnetometer-aided INS have been verified by covariance analysis using a simulated INS.

Introduction

A stand-alone inertial navigation system (INS) yields time-diverging solutions due to errors in the inertial measurement unit (IMU) sensors [1], that is accelerometers and rate-gyros arranged in their respective orthogonal triads. In myriad applications, such errors can preclude the use of the navigation solution in the long term. To circumvent this issue, a set of non-inertial sensors often aid the INS by means of a state-error model embedded in an extended Kalman filter [1]. The state-error model employs a state vector that comprises position and velocity errors, misalignment angles with respect to the locally horizontal coordinate frame, accelerometer biases, and rate-gyro drifts [1]. Consequently, observability analysis is called for to ensure that the filter estimates are accurate. Only with full observability the estimation error covariance can decrease to a minimum in all state-error space directions, and just then Kalman filter estimates can be used to correct the INS errors and calibrate the inertial sensors [2].

The state-error model is a time-varying, linear system, and thus observability matrix rank computation is not straightforward. For a stationary condition relative to the local coordinate frame, the state-error model becomes time-invariant. It has been known that in such case full observability is not achieved, and the Kalman filter does not work properly [1]. However, observability analysis of time-varying systems is much simplified under the assumption of piece-wise constant dynamics, in addition to the null space of the total observability matrix lying within the null space of the dynamics matrix in every distinct maneuver segment [3]. Then, full observability can be achieved by using velocity error measurements, and either accelerating the IMU in a specific manner [4], or by subjecting the IMU to some sort of rotation [5]. Further studies have tried to investigate observability without assuming piece-wise constant dynamics [6,7,8,9,10]. Since the observability analysis of time-varying systems is not easily applied under general conditions, several restrictions can be considered, for example, constant specific forces and angular velocities, or a C-shaped path [6,7,8,9,10].

Here constraints have been removed such as assuming a stationary vehicle, or alignment with the local horizontal frame. It is then shown that for almost all situations of interest and under the constraint of piece-wise constant dynamics, the observability analysis provides sufficient conditions for full observability that are general, and geometrically meaningful by use of concepts from linear algebra. Furthermore, to the best knowledge of the authors, the INS state-error model observability has not been studied in the case of magnetometer-aided INS.

Coordinate frames

The **true local horizontal frame** is used to represent the INS errors. In the true vehicle position, its X-axis points towards north, its Y-axis points towards east, and its Z-axis points down. This coordinate system is thereafter indicated with the *l* subscript.

[1] Ph.D. Student.
[2] Associate Professor.

The **computed coordinate frame** is defined as the local horizontal frame at the position computed by the INS. It is thereafter indicated with the *c* subscript.

The **platform coordinate frame** is defined as the local horizontal frame computed by the INS. It is thereafter indicated with the *p* subscript.

The **body coordinate frame** is defined as the sensors coordinate frame. It is usually assumed to be aligned with the vehicle coordinate frame in strapdown IMUs or aligned with the platform coordinate frame in IMUs mounted on a stabilized platform. This coordinate frame is thereafter indicated with the *b* subscript.

Notations and Abbreviations

$\Re$	The set of real numbers
DCM	Direction Cosine Matrix
y	Scalar
$\boldsymbol{y}$	Vector
$\boldsymbol{A}$	Matrix
$diag(\boldsymbol{A} \quad \boldsymbol{B} \quad \boldsymbol{C})$	Block-diagonal matrix constructed by the matrices $\boldsymbol{A}$, $\boldsymbol{B}$, and $\boldsymbol{C}$
$\boldsymbol{I}_n$	Identity matrix of size *n*
$[\boldsymbol{y}]_\times \boldsymbol{x}$	Matrix representation of the cross product $\boldsymbol{y} \times \boldsymbol{x}$
$\boldsymbol{D}_b^a$	Direction Cosine Matrix that rotates from the *a* coordinate frame to the *b* coordinate frame
$\boldsymbol{\omega}_c^{ab}$	Angular rate of the *a* coordinate frame with respect to the *b* coordinate frame represented in the *c* coordinate frame
$\boldsymbol{\rho}_l$	Transport rate represented in the local horizontal frame
$\boldsymbol{\Omega}_{e,l}$	Earth's angular rate represented in the local horizontal frame
$\boldsymbol{Asp}_l$	Specific force represented in the local horizontal frame
$\Delta\boldsymbol{R}_l$	INS position error represented in the local horizontal frame
$\Delta\boldsymbol{V}_l$	INS velocity error represented in the local horizontal frame
$\boldsymbol{\psi}$	Misalignment from the computed coordinate frame to the platform coordinate frame
∇	Bias of the accelerometers
$\boldsymbol{\varepsilon}$	Drift of the rate-gyros
R_N	North-south radius of curvature of the Earth
R_E	East-west radius of curvature of the Earth
R_e	Earth radius at the latitude of the vehicle
g_e	Gravitation at the latitude of the vehicle
λ	Latitude of the vehicle
h	Altitude of the vehicle
$\boldsymbol{\rho}_l + \boldsymbol{\Omega}_{e,l} = \boldsymbol{\omega}_l^{li}$	Angular rate of the local horizontal frame with respect to the inertial coordinate frame represented in the local horizontal frame

INS Error Model

INS errors are increasing and unbounded, thus navigation can be seriously compromised in a long-term mission even with high-quality inertial sensors [1,11]. To circumvent this problem, a set of non-inertial sensors provides additional information that can limit such errors. The fusion between the non-inertial sensors and the INS solution is often accomplished by an extended Kalman filter using a state-error model. Here, the state vector is composed of position and velocity errors, misalignment from the computed coordinate frame to the platform coordinate frame, bias of the accelerometers, and drift of the rate-gyros [11].

For the sake of completeness, the state-error model for an IMU mounted on a stabilized platform and a strapdown IMU are presented in Eqs. 1 and 2, respectively.

$$\dot{\boldsymbol{x}} = \begin{pmatrix} [\boldsymbol{\rho}_l]_\times & \boldsymbol{I}_3 & \boldsymbol{0}_3 & \boldsymbol{0}_3 & \boldsymbol{0}_3 \\ \boldsymbol{g}_e & \boldsymbol{\alpha} & \boldsymbol{\Gamma} & \boldsymbol{I}_3 & \boldsymbol{0}_3 \\ \boldsymbol{0}_3 & \boldsymbol{0}_3 & \boldsymbol{\beta} & \boldsymbol{0}_3 & -\boldsymbol{I}_3 \\ \boldsymbol{0}_3 & \boldsymbol{0}_3 & \boldsymbol{0}_3 & \boldsymbol{0}_3 & \boldsymbol{0}_3 \\ \boldsymbol{0}_3 & \boldsymbol{0}_3 & \boldsymbol{0}_3 & \boldsymbol{0}_3 & \boldsymbol{0}_3 \end{pmatrix} \boldsymbol{x}, \quad \boldsymbol{x} = \begin{bmatrix} \Delta\boldsymbol{R}_l^T & \Delta\boldsymbol{V}_l^T & \boldsymbol{\psi}^T & \nabla_l^T & \boldsymbol{\varepsilon}_l^T \end{bmatrix}^T; \tag{1}$$

$$\dot{\boldsymbol{x}} = \begin{pmatrix} [\boldsymbol{\rho}_l]_\times & \boldsymbol{I}_3 & \boldsymbol{0}_3 & \boldsymbol{0}_3 & \boldsymbol{0}_3 \\ \boldsymbol{g}_e & \boldsymbol{\alpha} & \boldsymbol{\Gamma} & \boldsymbol{D}_l^b & \boldsymbol{0}_3 \\ \boldsymbol{0}_3 & \boldsymbol{0}_3 & \boldsymbol{\beta} & \boldsymbol{0}_3 & -\boldsymbol{D}_l^b \\ \boldsymbol{0}_3 & \boldsymbol{0}_3 & \boldsymbol{0}_3 & \boldsymbol{0}_3 & \boldsymbol{0}_3 \\ \boldsymbol{0}_3 & \boldsymbol{0}_3 & \boldsymbol{0}_3 & \boldsymbol{0}_3 & \boldsymbol{0}_3 \end{pmatrix} \boldsymbol{x}, \quad \boldsymbol{x} = \begin{bmatrix} \Delta\boldsymbol{R}_l^T & \Delta\boldsymbol{V}_l^T & \boldsymbol{\psi}^T & \nabla_b^T & \boldsymbol{\varepsilon}_b^T \end{bmatrix}^T, \tag{2}$$

where $\boldsymbol{g}_e = diag\left(-g_e/R_e \quad -g_e/R_e \quad 2g_e/R_e\right)$, $\boldsymbol{\alpha} = [\boldsymbol{\rho}_l + 2\boldsymbol{\Omega}_{e,l}]_\times$, $\boldsymbol{\beta} = [\boldsymbol{\rho}_l + \boldsymbol{\Omega}_{e,l}]_\times$, and $\boldsymbol{\Gamma} = [\boldsymbol{Asp}]_\times$. Furthermore, a third model is constructed by applying the Lyapunov transformation [6] in Eq. 3 to model 2. The result is presented in Eq. 4.

$$\boldsymbol{P}(t) = \begin{pmatrix} \boldsymbol{I}_3 & \boldsymbol{0}_3 & \boldsymbol{0}_3 & \boldsymbol{0}_3 & \boldsymbol{0}_3 \\ \boldsymbol{0}_3 & \boldsymbol{I}_3 & \boldsymbol{0}_3 & \boldsymbol{0}_3 & \boldsymbol{0}_3 \\ \boldsymbol{0}_3 & \boldsymbol{0}_3 & \boldsymbol{I}_3 & \boldsymbol{0}_3 & \boldsymbol{0}_3 \\ \boldsymbol{0}_3 & \boldsymbol{0}_3 & \boldsymbol{0}_3 & \boldsymbol{D}_l^b & \boldsymbol{0}_3 \\ \boldsymbol{0}_3 & \boldsymbol{0}_3 & \boldsymbol{0}_3 & \boldsymbol{0}_3 & \boldsymbol{D}_l^b \end{pmatrix}; \tag{3}$$

$$\dot{\boldsymbol{x}} = \begin{pmatrix} [\boldsymbol{\rho}_l]_\times & \boldsymbol{I}_3 & \boldsymbol{0}_3 & \boldsymbol{0}_3 & \boldsymbol{0}_3 \\ \boldsymbol{g}_e & \boldsymbol{\alpha} & \boldsymbol{\Gamma} & \boldsymbol{I}_3 & \boldsymbol{0}_3 \\ \boldsymbol{0}_3 & \boldsymbol{0}_3 & \boldsymbol{\beta} & \boldsymbol{0}_3 & -\boldsymbol{I}_3 \\ \boldsymbol{0}_3 & \boldsymbol{0}_3 & \boldsymbol{0}_3 & \boldsymbol{\omega}^* & \boldsymbol{0}_3 \\ \boldsymbol{0}_3 & \boldsymbol{0}_3 & \boldsymbol{0}_3 & \boldsymbol{0}_3 & \boldsymbol{\omega}^* \end{pmatrix} \boldsymbol{x}, \quad \boldsymbol{x} = \begin{bmatrix} \Delta\boldsymbol{R}_l^T & \Delta\boldsymbol{V}_l^T & \boldsymbol{\psi}^T & \nabla_l^T & \boldsymbol{\varepsilon}_l^T \end{bmatrix}^T, \tag{4}$$

where $\boldsymbol{\omega}^* = [\boldsymbol{\omega}_l^{bl}]_\times$.

If the observables directly measure the position and velocity errors, then, by definition, those state vector components are observable. The position error is dynamically coupled only with the velocity error, which shows that the position error dynamics fails to bring any unmeasured component into the observable subspace. Hence, for the sake of simplicity of the observability analysis, the position error component can be neglected [2]. The models in Eqs. 1, 2, and 4 without the position error are thereafter called models 1, 2, and 3, respectively.

Since model 3 relates to model 2 by a Lyapunov transformation that preserves observability, then it is clear that model 3 with a set of sensors is fully observable if and only if the same condition holds for model 2 with the same set of sensors.

Non-inertial sensors measurement model

This investigation concentrates on INS error-state observability analysis when three distinct non-inertial sensors aid the INS: GPS, magnetometer, and camera. A measurement model for each one is described next.

The GPS observables are assumed to directly provide position and velocity errors. In practice, GPS raw data can be post-processed to yield vehicle position and velocity in the WGS84 ellipsoid coordinate frame as in a loosely-coupled implementation. Alternatively, the raw data composed of, for example, pseudo-ranges and Doppler shift between the receiver and the satellites are employed in a tightly-coupled implementation [11]. The GPS observables are then compared to the INS solution to produce a measurement vector of the state-error. Receiver clock errors have not been involved in this investigation.

The GPS measurement equation under the aforementioned assumption and neglecting measurement noise is presented in Eq. 5.

$$\boldsymbol{y}_{GPS} = \begin{bmatrix} \boldsymbol{I}_3 & \boldsymbol{0}_3 & \boldsymbol{0}_3 & \boldsymbol{0}_3 & \boldsymbol{0}_3 \\ \boldsymbol{0}_3 & \boldsymbol{I}_3 & \boldsymbol{0}_3 & \boldsymbol{0}_3 & \boldsymbol{0}_3 \end{bmatrix} \boldsymbol{x}. \tag{5}$$

The magnetometer observables are composed of the difference between the magnetometer raw data and the INS-based local geomagnetic field vector. Considering Pinson's model [12], the DCM from the body coordinate frame to the true local horizontal frame can be approximated by neglecting second order terms as in Eq. 6.

$$\boldsymbol{D}_b^l = \boldsymbol{D}_b^p \cdot \boldsymbol{D}_p^c \cdot \boldsymbol{D}_c^l = \boldsymbol{D}_b^p \cdot (\boldsymbol{I}_3 - [\boldsymbol{\psi}]_\times) \cdot (\boldsymbol{I}_3 - [\Delta\boldsymbol{\theta}]_\times) \approx \boldsymbol{D}_b^p \cdot (\boldsymbol{I}_3 - [\boldsymbol{\psi}]_\times - [\Delta\boldsymbol{\theta}]_\times), \tag{6}$$

where $\Delta\boldsymbol{\theta}$ is the misalignment from the true coordinate frame to the computed coordinate frame and $\boldsymbol{\psi}$ is misalignment from the computed coordinate frame to the platform coordinate frame. Thus, the magnetometer measurement neglecting noise can be approximated by:

$$\mathbf{B}_{mag} \approx \mathbf{D}_b^p \cdot (\mathbf{I}_3 - [\psi]_\times - [\Delta\theta]_\times)\mathbf{B}_l \Rightarrow \mathbf{B}_{mag} - \mathbf{D}_b^p \mathbf{B}_l \approx -\mathbf{D}_b^p [\psi]_\times \mathbf{B}_l - \mathbf{D}_b^p [\Delta\theta]_\times \mathbf{B}_l$$
$$\mathbf{D}_p^b \mathbf{B}_{mag} - \mathbf{B}_l \approx -[\psi]_\times \mathbf{B}_l - [\Delta\theta]_\times \mathbf{B}_l \tag{7}$$
$$\mathbf{y}_{mag} = [\mathbf{B}_l]_\times \psi + [\mathbf{B}_l]_\times \Delta\theta$$

where $\boldsymbol{B}_{mag}$ is the raw magnetometer measurement and $\boldsymbol{B}_l$ is the local geomagnetic field vector represented in the true local horizontal frame, which is not accessible. The latter is usually obtained from a geomagnetic field model using the position solution either computed by the GPS or by the INS. It is straightforward to check that $\boldsymbol{D}_b^p = \boldsymbol{I}_3$ if the IMU and the magnetometer are mounted on a stabilized platform. Moreover, vector $\boldsymbol{\Delta\theta}$ can be related to the position error represented in the local horizontal frame as in Eq. 8.

$$\boldsymbol{\Delta\theta} = \begin{bmatrix} 0 & \frac{1}{R_E + h} & 0 \\ -\frac{1}{R_N + h} & 0 & 0 \\ 0 & \frac{\tan\lambda}{R_E + h} & 0 \end{bmatrix} \boldsymbol{\Delta R}_l = \boldsymbol{C} \cdot \boldsymbol{\Delta R}_l \,. \tag{8}$$

Finally, the magnetometer measurement can be approximated by:

$$\boldsymbol{y}_{mag} = \begin{bmatrix} \boldsymbol{C} \cdot [\boldsymbol{B}_l]_\times & \boldsymbol{0}_3 & [\boldsymbol{B}_l]_\times & \boldsymbol{0}_3 & \boldsymbol{0}_3 \end{bmatrix} \boldsymbol{x} \,. \tag{9}$$

The camera observables are assumed to directly measure the position error and misalignment from the computed coordinate frame to the platform coordinate frame [14]. According to the approach described in [14], this assumption is true if the camera can track a minimum number (≥ 3) of landmarks at the same time. Thus the camera measurement equation is presented in Eq. 10:

$$\boldsymbol{y}_{cam} = \begin{bmatrix} \boldsymbol{L}_3 & \boldsymbol{0}_3 & \boldsymbol{0}_3 & \boldsymbol{0}_3 & \boldsymbol{0}_3 \\ \boldsymbol{0}_3 & \boldsymbol{0}_3 & \boldsymbol{J}_3 & \boldsymbol{0}_3 & \boldsymbol{0}_3 \end{bmatrix} \boldsymbol{x} \,, \tag{10}$$

where $\boldsymbol{L}_3$ and $\boldsymbol{J}_3$ are full rank matrices [14].

Observability analysis of piece-wise constant systems

From the INS error dynamics in Eqs. 1, 2, and, 4, one concludes that it is a time-varying, linear system. The most general way to check observability is to compute the observability Grammian [13]. However, it leads to such complicated mathematical treatment that it is unfeasible for the addressed problem.

In the literature, observability has been verified by three main methods. The first is to analyze conditions that turn the model into a time-invariant system, e. g. the vehicle is stationary on the Earth's surface, or to find an adequate Lyapunov transformation that also leads to a time-invariant system. Thus the observability can be checked by means of rank computation of the observability matrix [13]. This approach was used in [1,6].

The second method is applicable to piece-wise constant (PWC) systems. The observability analysis is still done by rank computation, but it turns out that it can be greatly simplified when a certain condition holds as is presented in Theorem 1[3]. For the INS error model 1, the system can be considered PWC if the specific force is piece-wise constant [4]. For the INS error model 2, the system can be approximated by a PWC system if the specific force and attitude with respect to the local horizontal frame are piece-wise constant [5]. Finally, for the INS error model 3, the PWC system assumption holds if the specific force and IMU angular rate with respect to the local horizontal frame and represented in this frame are piece-wise constant.

The third method has tried to investigate observability without assuming piece-wise constant dynamics [6,7,8,9,10]. Since the observability analysis of time-varying systems is not easily applied under general conditions, several restrictions can be considered, for example, constant specific forces and angular velocities, or a C-shaped path.

For the sake of simplicity, the second method based on assuming piece-wise constant dynamics has been preferred here. It can be shown that under this constraint, an observability analysis with linear algebra concepts provides sufficient conditions for full observability that hold for practically all situations of interest. Additionally, the approach yields a geometrical insight of the kinematics involved in the observability analysis. Let a vehicle move at constant altitude according to three consecutive trajectory segments: 1) towards North; 2)

in a C-shaped trajectory; and 3) towards East. The composed movement leads to a time-varying INS error model. However, if segment 2 is neglected, then the above INS error models turn into PWC systems. Thus, if full observability by the end of segment 3 can be proved, then, by definition, the time-varying system composed of the three segments is also fully observable. However, if full observability cannot be claimed from the analysis of the first and the third PWC segments, then further analysis including the second segment is needed. For practically all the situations of interest, the vehicle can move in such a manner that the INS error model will remain constant during certain time intervals. Thus the analysis of just these segments using the aforementioned method can provide **sufficient conditions** for full observability.

A PWC system is defined as in Eq. 11:

$$\begin{aligned} \dot{\boldsymbol{x}} &= \boldsymbol{A}_j \boldsymbol{x} + \boldsymbol{B}_j \boldsymbol{u} \\ \boldsymbol{y} &= \boldsymbol{C}_j \boldsymbol{x} \end{aligned} \tag{11}$$

where $j \in [0,1,2,3,...]$ and matrices $\boldsymbol{A}_j$, $\boldsymbol{B}_j$, and $\boldsymbol{C}_j$ are constant for all j. Observability can be checked by rank analysis of the total observability matrix (TOM), defined as in Eq. 12 for the first r segments [3]:

$$\overline{\boldsymbol{Q}}(r) = \left[\left[\overline{\boldsymbol{Q}}_0\right]^T \quad \left[\overline{\boldsymbol{Q}}_1 \cdot e^{\boldsymbol{A}_0 \boldsymbol{\Delta}_0}\right]^T \quad \cdots \quad \left[\overline{\boldsymbol{Q}}_i \cdot \prod_{k=i-1}^{0} e^{\boldsymbol{A}_k \boldsymbol{\Delta}_k}\right]^T \quad \cdots \quad \left[\overline{\boldsymbol{Q}}_r \cdot \prod_{k=r-1}^{0} e^{\boldsymbol{A}_k \boldsymbol{\Delta}_k}\right]^T \right]^T \tag{12}$$

Matrix $\overline{\boldsymbol{Q}}_i$ is defined as in Eq. 13:

$$\overline{\boldsymbol{Q}}_i = \left[\left[\boldsymbol{C}_i\right]^T \quad \left[\boldsymbol{C}_i \boldsymbol{A}_i\right]^T \quad \left[\boldsymbol{C}_i \boldsymbol{A}_i^2\right]^T \quad \cdots \quad \left[\boldsymbol{C}_i \boldsymbol{A}_i^{n-1}\right]^T \right] \tag{13}$$

where n is the state vector dimension. The computation of the exponential matrices leads to tedious and complicated algebraic calculations, but it can be avoided if the following theorem holds [3].

Theorem 1 [3]: If:

$$NULL(\overline{\boldsymbol{Q}}_i) \subset NULL(\boldsymbol{A}_i), \quad \forall j \in [0,1,2,3,\cdots,r]$$

then the following holds:

$$\begin{aligned} NULL(\overline{\boldsymbol{Q}}(r)) &= NULL(\overline{\boldsymbol{Q}}_s(r)) \\ RANK(\overline{\boldsymbol{Q}}(r)) &= RANK(\overline{\boldsymbol{Q}}_s(r)) \end{aligned}$$

where $\overline{\boldsymbol{Q}}_s(r)$ is the stripped observability matrix (SOM) defined as in Eq. 14:

$$\overline{\boldsymbol{Q}}_s(r) = \left[\left[\overline{\boldsymbol{Q}}_0\right]^T \quad \left[\overline{\boldsymbol{Q}}_1\right]^T \quad \cdots \quad \left[\overline{\boldsymbol{Q}}_i\right]^T \quad \cdots \quad \left[\overline{\boldsymbol{Q}}_r\right]^T \right]^T \tag{14}$$

Thus the computation of the exponential matrices can be avoided. The proof can be found in [3].

The validity of Theorem 1 for model 1 with GPS measurements was shown in [4]. However, further analysis brings out a novel condition that should be satisfied. The observability matrix for the j-th segment can be written, after elementary row operations, as in Eq. 15:

$$\overline{\boldsymbol{Q}}_j' = \left[\begin{array}{cccc|c} \boldsymbol{I}_3 & \boldsymbol{0}_3 & \boldsymbol{0}_3 & \boldsymbol{0}_3 & Line\ 1 \\ \boldsymbol{0}_3 & \boldsymbol{\Gamma}_j & \boldsymbol{I}_3 & \boldsymbol{0}_3 & Line\ 2 \\ \boldsymbol{0}_3 & \boldsymbol{\Gamma}_j\boldsymbol{\beta} & \boldsymbol{0}_3 & -\boldsymbol{\Gamma}_j & Line\ 3 \\ \vdots & \vdots & \vdots & \vdots & \vdots \\ \boldsymbol{0}_3 & \boldsymbol{\Gamma}_j\boldsymbol{\beta}^{n-2} & \boldsymbol{0}_3 & \boldsymbol{\Gamma}_j\boldsymbol{\beta}^{n-3} & Line\ n \\ \vdots & \vdots & \vdots & \vdots & \vdots \end{array}\right] \tag{15}$$

where the subscript j indicates the specific force at j-th segment and $Line\ n$ are properly sized blocks. Notice that matrix $\boldsymbol{\beta}$, which is the cross product matrix of the angular rate vector $\boldsymbol{\omega}_l^{li}$, is time-varying. However, $\boldsymbol{\beta}$ can be approximated as a constant for a short term analysis if the terrestrial speed is small enough.

A vector $\boldsymbol{x} \in NULL(\overline{\boldsymbol{Q}}_j')$ must satisfy the following conditions:

$$(1)\ \boldsymbol{x}_1 = \boldsymbol{0}_{3\times1} \qquad (2)\ \boldsymbol{\Gamma}_j\boldsymbol{x}_2 + \boldsymbol{x}_3 = \boldsymbol{0}_{3\times1} \qquad (3)\ \boldsymbol{\Gamma}_j\boldsymbol{\beta}_j^n(\boldsymbol{\beta}_j\boldsymbol{x}_2 - \boldsymbol{x}_4) = \boldsymbol{0}_{3\times1},\ n = [0,1,2,\cdots] \tag{16}$$

A priori, one cannot claim whether $\boldsymbol{x}$ lies or not in $NULL(\boldsymbol{A}_j)$. However, if $\boldsymbol{Asp}_{l,j}$ is not aligned with $\boldsymbol{\omega}_l^{li}$, then the third condition and Theorem A.4 leads to $\boldsymbol{\beta}_j\boldsymbol{x}_2 - \boldsymbol{x}_4 = \boldsymbol{0}_{3\times1}$. Thus, it can be verified that $\boldsymbol{x}$ also lies in $NULL(\boldsymbol{A}_j)$ using the same procedure as in [4].

For model 2 using GPS measurements, [5] verified that Theorem 1 remains valid. However the authors omitted the same restriction as above: that Theorem 1 is only valid if $\boldsymbol{Asp}_{l,j}$ is not aligned with $\boldsymbol{\omega}_l^{li}$. The verification is straightforward and will be omitted here for the sake of space.

In case an additional sensor is added to GPS measurements, then it is trivial to check the validity of Theorem 1 for models 1 and 2. However, recent results have shown that the use of an additional sensor allows for the relaxation of the aforementioned restriction about the required misalignment of $\boldsymbol{Asp}_{l,j}$ and $\boldsymbol{\omega}_l^{li}$ [15].

As a result, the observability analysis of models 1 and 2 with GPS measurements can be performed by means of SOM rank computation if the specific force $\boldsymbol{Asp}_{l,j}$ at any segment is not aligned with the angular rate of the local horizontal frame with respect to the inertial coordinate frame $\boldsymbol{\omega}_l^{li}$.

Observability Analysis: IMU mounted on a locally horizontal-stabilized platform in a GPS-aided INS

This scenario was already analyzed in [4]. It was proved that full observability is achieved if the movement is composed of, at least, three distinct specific force segments selected from table I in [4]. However, it has not been shown how these segments can be constructed. This extension is developed next.

The SOM for the first three segments can be assembled after elementary row and column operations as in Eq. 17a. Additionally, a vector $\boldsymbol{x} \in NULL(\overline{\boldsymbol{Q}}_s'(2))$ must satisfy the conditions in Eq. 17b.

$$\overline{\boldsymbol{Q}}_s'(2) = \begin{bmatrix} \boldsymbol{I}_3 & \boldsymbol{0}_3 & \boldsymbol{0}_3 & \boldsymbol{0}_3 \\ \boldsymbol{0}_3 & \boldsymbol{0}_3 & \boldsymbol{I}_3 & \boldsymbol{0}_3 \\ \boldsymbol{0}_3 & \boldsymbol{0}_3 & \boldsymbol{0}_3 & -\boldsymbol{\Gamma}_0 \\ \boldsymbol{0}_3 & \boldsymbol{0}_3 & \boldsymbol{0}_3 & -\boldsymbol{\Gamma}_0\boldsymbol{\beta} \\ \boldsymbol{0}_3 & \boldsymbol{\Gamma}_1 - \boldsymbol{\Gamma}_0 & \boldsymbol{0}_3 & \boldsymbol{0}_3 \\ \boldsymbol{0}_3 & \boldsymbol{0}_3 & \boldsymbol{0}_3 & -\boldsymbol{\Gamma}_1 \\ \boldsymbol{0}_3 & \boldsymbol{0}_3 & \boldsymbol{0}_3 & -\boldsymbol{\Gamma}_1\boldsymbol{\beta} \\ \boldsymbol{0}_3 & \boldsymbol{\Gamma}_2 - \boldsymbol{\Gamma}_0 & \boldsymbol{0}_3 & \boldsymbol{0}_3 \\ \boldsymbol{0}_3 & \boldsymbol{0}_3 & \boldsymbol{0}_3 & -\boldsymbol{\Gamma}_2 \\ \boldsymbol{0}_3 & \boldsymbol{0}_3 & \boldsymbol{0}_3 & -\boldsymbol{\Gamma}_2\boldsymbol{\beta} \\ \vdots & \vdots & \vdots & \vdots \end{bmatrix} \tag{17a}$$

$$\begin{cases} 1) & \boldsymbol{x}_1 = \boldsymbol{0}_{3\times1} \\ 2) & \boldsymbol{x}_3 = \boldsymbol{0}_{3\times1} \\ 3) & (\boldsymbol{\Gamma}_1 - \boldsymbol{\Gamma}_0)\boldsymbol{x}_2 = \boldsymbol{0}_{3\times1} \\ 4) & (\boldsymbol{\Gamma}_2 - \boldsymbol{\Gamma}_0)\boldsymbol{x}_2 = \boldsymbol{0}_{3\times1} \\ 5) & \boldsymbol{\Gamma}_0\boldsymbol{\beta}^n\boldsymbol{x}_4 = \boldsymbol{0}_{3\times1}, \quad n \in [0,1] \\ 6) & \boldsymbol{\Gamma}_1\boldsymbol{\beta}^n\boldsymbol{x}_4 = \boldsymbol{0}_{3\times1}, \quad n \in [0,1] \\ 7) & \boldsymbol{\Gamma}_2\boldsymbol{\beta}^n\boldsymbol{x}_4 = \boldsymbol{0}_{3\times1}, \quad n \in [0,1] \end{cases} \tag{17b}$$

The remaining lines do not convey relevant information for the analysis. Since Theorem 1 must hold for this analysis, then the specific force $\boldsymbol{Asp}_{l,j}$ cannot be aligned with the angular rate of the local horizontal frame with respect to the inertial coordinate frame $\boldsymbol{\omega}_l^{li}$. Thus, conditions 5, 6, and 7 in Eq. 17b together with Theorem A.4 yield $\boldsymbol{x}_4 = \boldsymbol{0}_{3\times1}$. Moreover, condition 3 and Theorem A.1 claim that $\boldsymbol{x}_2$ must lie in the one-dimensional subspace defined by the vector difference $\boldsymbol{Asp}_{l,1} - \boldsymbol{Asp}_{l,0}$. Likewise, condition 4 also restricts $\boldsymbol{x}_2$ and

$\boldsymbol{Asp}_{l,2} - \boldsymbol{Asp}_{l,0}$ to be linearly dependent vectors. Thus, if $\boldsymbol{Asp}_{l,1} - \boldsymbol{Asp}_{l,0}$ is not aligned with $\boldsymbol{Asp}_{l,2} - \boldsymbol{Asp}_{l,0}$, then full observability is achieved. One can note that the three different segments in table I in [4] satisfy the conditions in Eq. 17b.

Observability Analysis: IMU mounted on a locally horizontal-stabilized platform in a GPS/Magnetometer-aided INS

It is shown in what follows that by using a calibrated magnetometer the number of segments needed to achieve full observability is reduced by one. In this scenario, the segments differ from each other only in the specific force vector because the local geomagnetic field vector represented in the local horizontal frame is assumed to remain constant for a short term analysis. Thus, the SOM for the first two segments can be written after elementary row and column operations as in Eq. 18a. Additionally, a vector $\boldsymbol{x} \in NULL(\overline{\boldsymbol{Q}}_s'(2))$ must satisfy the conditions in Eq. 18b.

$$\overline{\boldsymbol{Q}}_s'(2) = \begin{bmatrix} \boldsymbol{I}_3 & \boldsymbol{0}_3 & \boldsymbol{0}_3 & \boldsymbol{0}_3 \\ \boldsymbol{0}_3 & \boldsymbol{0}_3 & \boldsymbol{I}_3 & \boldsymbol{0}_3 \\ \boldsymbol{0}_3 & \boldsymbol{0}_3 & \boldsymbol{0}_3 & -\boldsymbol{\Gamma}_0 \\ \boldsymbol{0}_3 & \boldsymbol{0}_3 & \boldsymbol{0}_3 & -\boldsymbol{\Gamma}_0\boldsymbol{\beta} \\ \boldsymbol{0}_3 & \boldsymbol{\Gamma}_1 - \boldsymbol{\Gamma}_0 & \boldsymbol{0}_3 & \boldsymbol{0}_3 \\ \boldsymbol{0}_3 & \boldsymbol{0}_3 & \boldsymbol{0}_3 & -\boldsymbol{\Gamma}_1 \\ \boldsymbol{0}_3 & \boldsymbol{0}_3 & \boldsymbol{0}_3 & -\boldsymbol{\Gamma}_1\boldsymbol{\beta} \\ \boldsymbol{0}_3 & \boldsymbol{B}_l & \boldsymbol{0}_3 & \boldsymbol{0}_3 \\ \boldsymbol{0}_3 & \boldsymbol{0}_3 & \boldsymbol{0}_3 & -[\boldsymbol{B}_l]_\times \\ \boldsymbol{0}_3 & \boldsymbol{0}_3 & \boldsymbol{0}_3 & -[\boldsymbol{B}_l]_\times\boldsymbol{\beta} \\ \vdots & \vdots & \vdots & \vdots \end{bmatrix} \tag{18a}$$

$$\begin{cases} 1) & \boldsymbol{x}_1 = \boldsymbol{0}_{3\times1} \\ 2) & \boldsymbol{x}_3 = \boldsymbol{0}_{3\times1} \\ 3) & (\boldsymbol{\Gamma}_1 - \boldsymbol{\Gamma}_0)\boldsymbol{x}_2 = \boldsymbol{0}_{3\times1} \\ 4) & [\boldsymbol{B}_l]_\times \boldsymbol{x}_2 = \boldsymbol{0}_{3\times1} \\ 5) & \boldsymbol{\Gamma}_0\boldsymbol{\beta}^n\boldsymbol{x}_4 = \boldsymbol{0}_{3\times1}, \quad n \in [0,1] \\ 6) & \boldsymbol{\Gamma}_1\boldsymbol{\beta}^n\boldsymbol{x}_4 = \boldsymbol{0}_{3\times1}, \quad n \in [0,1] \\ 7) & [\boldsymbol{B}_l]_\times\boldsymbol{\beta}^n\boldsymbol{x}_4 = \boldsymbol{0}_{3\times1}, \quad n \in [0,1] \end{cases} \tag{18b}$$

Conditions 5, 6, and 7 in Eq. 18b together with Theorem A.4 yield $\boldsymbol{x}_4 = \boldsymbol{0}_{3\times1}$ as in the previous analysis. Furthermore, conditions 3 and 4 restrict $\boldsymbol{x}_2$ to be simultaneously aligned to the local geomagnetic field vector $\boldsymbol{B}_l$ and the vector difference $\boldsymbol{Asp}_{l,1} - \boldsymbol{Asp}_{l,0}$. Thus, if these two vectors are not aligned, then the only possible solution for $\boldsymbol{x}_2$ is $\boldsymbol{0}_{3\times1}$. Therefore, the SOM null space has dimension zero and the system is fully observable. In other words, if the IMU is mounted on a locally horizontal-stabilized platform in a GPS/Magnetometer-aided INS, then full observability is achieved if there are at least two segments in which the corresponding specific force difference $\boldsymbol{Asp}_{l,1} - \boldsymbol{Asp}_{l,0}$ is not aligned with the local geomagnetic field vector $\boldsymbol{B}_l$.

If the magnetometer is not calibrated, e.g. if the observables have an unknown bias, then the above result does not hold and further investigation is necessary.

Observability Analysis: IMU mounted on a locally horizontal-stabilized platform in a GPS/Camera-aided INS

The observability matrix for the first segment can be written after elementary row and column operations as in Eq. 19:

$$\overline{\boldsymbol{Q}}_0' = \begin{bmatrix} \boldsymbol{I}_3 & \boldsymbol{0}_3 & \boldsymbol{0}_3 & \boldsymbol{0}_3 \\ \boldsymbol{0}_3 & \boldsymbol{J}_3 & \boldsymbol{0}_3 & \boldsymbol{0}_3 \\ \boldsymbol{0}_3 & \boldsymbol{0}_3 & \boldsymbol{I}_3 & \boldsymbol{0}_3 \\ \boldsymbol{0}_3 & \boldsymbol{0}_3 & \boldsymbol{0}_3 & -\boldsymbol{J}_3 \\ \vdots & \vdots & \vdots & \vdots \end{bmatrix} \tag{19}$$

where J3 is a full rank matrix as referred to in Eq. 10. Hence $\overline{\boldsymbol{Q}}_0'$ is a full rank matrix, and thus the INS error model is fully observable from the onset of the first segment when GPS and camera measurements are available.

Observability Analysis: Strapdown IMU in a GPS-aided INS

By analyzing model 3, one can note that the INS error model dynamics of a strapdown IMU is equal to the model of an IMU mounted on a stabilized platform if the IMU angular rate with respect to the local horizontal frame $\boldsymbol{\omega}_l^{bl}$ is zero. In such case, the previous results of the observability analysis regarding an IMU mounted on a stabilized platform remain valid. Moreover, the INS error model of a strapdown IMU can be also stimulated by rotational motion. Thus additional excitation signals are available to increase the dimension of the observable subspace. The analysis of the scenario in which the IMU undergoes PWC attitude is presented next.

The observable subspace dimension was first investigated in [5] considering that the IMU position was stationary on Earth's surface though subjected to consecutive rotations. [6] proposed to rotate a stationary IMU with a constant angular rate with respect to the local frame and verified that if the angular rate vector satisfies a set of conditions, then full observability is achieved. Moreover, [7] analyzed a more general situation that circumvents the need for the IMU to remain stationary, although the conditions for full observability are not easily grasped geometrically and it is not straightforward to claim whether a specific trajectory segment leads to full observability.

From Eq. 2, the observability matrix of the model 2 for the first two segments can be written after elementary row and column operations as in Eq. 20a. Additionally, a vector $\boldsymbol{x} \in NULL(\overline{\boldsymbol{Q}}_s'(1))$ must satisfy the conditions in Eq. 20b.

$$\overline{\boldsymbol{Q}}_s'(1) = \begin{bmatrix} \boldsymbol{I}_3 & \boldsymbol{0}_3 & \boldsymbol{0}_3 & \boldsymbol{0}_3 \\ \boldsymbol{0}_3 & \boldsymbol{\Gamma}_0 & \boldsymbol{D}_l^{b0} & \boldsymbol{0}_3 \\ \boldsymbol{0}_3 & \boldsymbol{\Gamma}_0\boldsymbol{\beta} & \boldsymbol{0}_3 & -\boldsymbol{\Gamma}_0\boldsymbol{D}_l^{b0} \\ \boldsymbol{0}_3 & \boldsymbol{\Gamma}_0\boldsymbol{\beta}^2 & \boldsymbol{0}_3 & -\boldsymbol{\Gamma}_0\boldsymbol{\beta}\boldsymbol{D}_l^{b0} \\ \boldsymbol{0}_3 & \boldsymbol{0}_3 & \boldsymbol{D}_l^{b1} - \boldsymbol{D}_l^{b0} & \boldsymbol{0}_3 \\ \boldsymbol{0}_3 & \boldsymbol{0}_3 & \boldsymbol{0}_3 & \boldsymbol{\Gamma}_0(\boldsymbol{D}_l^{b1} - \boldsymbol{D}_l^{b0}) \\ \boldsymbol{0}_3 & \boldsymbol{0}_3 & \boldsymbol{0}_3 & \boldsymbol{\Gamma}_0\boldsymbol{\beta}(\boldsymbol{D}_l^{b1} - \boldsymbol{D}_l^{b0}) \\ \vdots & \vdots & \vdots & \vdots \end{bmatrix} \tag{20a}$$

$$\begin{cases} 1) \quad \boldsymbol{x}_1 = \boldsymbol{0}_{3\times1} \\ 2) \quad \boldsymbol{\Gamma}_0\boldsymbol{x}_2 + \boldsymbol{D}_l^{b0}\boldsymbol{x}_3 = \boldsymbol{0}_{3\times1} \\ 3) \quad \boldsymbol{\Gamma}_0\boldsymbol{\beta}^n(\boldsymbol{\beta}\boldsymbol{x}_2 - \boldsymbol{D}_l^{b0}\boldsymbol{x}_4) = \boldsymbol{0}_{3\times1},\ n \in [0,1] \\ 4) \quad (\boldsymbol{D}_l^{b1} - \boldsymbol{D}_l^{b0})\boldsymbol{x}_3 = \boldsymbol{0}_{3\times1} \\ 5) \quad \boldsymbol{\Gamma}_0\boldsymbol{\beta}^n(\boldsymbol{D}_l^{b1} - \boldsymbol{D}_l^{b0})\boldsymbol{x}_4 = \boldsymbol{0}_{3\times1},\ n \in [0,1] \end{cases} \tag{20b}$$

where superscripts *b0* and *b1* indicate, respectively, the body coordinate frames at an instant in segment 0 and at another instant in segment 1. Additionally, it is assumed that the terrestrial speed is such that the local horizontal frame remains almost constant between segments 0 and 1.

If the specific force $\boldsymbol{Asp}_{l,0}$ and the angular rate of the local horizontal frame with respect to the inertial coordinate frame $\boldsymbol{\omega}_l^{li}$ are not aligned, which must be true for the validity of Theorem 1, then Theorem A.4 together with conditions 3 and 5 in Eq. 20b lead to (a) $\boldsymbol{\beta}\boldsymbol{x}_2 - \boldsymbol{D}_l^{b0}\boldsymbol{x}_4 = \boldsymbol{0}_{3\times1}$ and (b) $(\boldsymbol{D}_l^{b1} - \boldsymbol{D}_l^{b0})\boldsymbol{x}_4 = \boldsymbol{0}_{3\times1}$. Condition (b) together with Theorem A.6 claim that $\boldsymbol{x}_4$ must lie in the Euler axis in which a single rotation aligns the *b0* coordinate frame with the *b1* coordinate frame. This axis is thereafter called $\boldsymbol{e}_{b0\leftrightarrow b1}$. Likewise, $\boldsymbol{x}_3$ must also lie in the same axis due to condition 4. Then condition 2 leads to $\boldsymbol{\Gamma}_0\boldsymbol{x}_2 = -\boldsymbol{D}_l^{b0}\boldsymbol{x}_3$, which constrains

$\boldsymbol{x}_2$ and the specific force $\boldsymbol{Asp}_{l,0}$ to lie in a plane perpendicular to the Euler axis $\boldsymbol{e}_{b0\leftrightarrow b1}$ if $\boldsymbol{x}_3$ is not $\boldsymbol{0}_{3\times1}$. In the same way, if $\boldsymbol{x}_4$ is not $\boldsymbol{0}_{3\times1}$, then condition (a) above constrains $\boldsymbol{x}_2$ and the angular rate of the local horizontal frame with respect to the inertial coordinate frame $\boldsymbol{\omega}_l^{li}$ to also lie in a plane perpendicular to the same Euler axis $\boldsymbol{e}_{b0\leftrightarrow b1}$. Hence, if either the specific force $\boldsymbol{Asp}_{l,0}$ **or** the angular rate of the local horizontal frame with respect to the inertial coordinate frame $\boldsymbol{\omega}_l^{li}$ is not perpendicular to the Euler axis $\boldsymbol{e}_{b0\leftrightarrow b1}$, then the only possible solution for $\boldsymbol{x}$ in the null space is that the components $\boldsymbol{x}_2$, $\boldsymbol{x}_3$, and $\boldsymbol{x}_4$ are all $\boldsymbol{0}_{3\times1}$. In such case, $\overline{\boldsymbol{Q}}_s'(1)$ yields a null space whose dimension is zero. In other words, if either $\boldsymbol{Asp}_{l,0}$ or $\boldsymbol{\omega}_l^{li}$ is not perpendicular to the Euler axis $\boldsymbol{e}_{b0\leftrightarrow b1}$, which otherwise would be a rather particular coincidence that would not likely endure during an usual trajectory, then the INS error model is fully observable.

The foregoing conclusion is in agreement with the results in [5], but provides much more general conditions to verify observability. The investigation in [5] focused on INS error model observability of a stationary vehicle when the IMU was initially pointing towards North and then subjected to PWC attitude changes. It was concluded that IMU rotation about either the North or the local vertical axis yields full observability. However, a rotation about the East axis was not enough to achieve full observability. Indeed, from the above analysis, one notes that for a stationary vehicle (no matter where it points to), $\boldsymbol{Asp}_{l,0}$ and $\boldsymbol{\omega}_l^{li}$ lie in the plane spanned by the local North and vertical directions, and a single rotation about the East axis gives the Euler axis $\boldsymbol{e}_{b0\leftrightarrow b1}$ aligned with the East. Thus $\boldsymbol{e}_{b0\leftrightarrow b1}$ is simultaneously perpendicular to $\boldsymbol{Asp}_{l,0}$ and $\boldsymbol{\omega}_l^{li}$, and hence the INS error model is not fully observable.

Observability Analysis: Strapdown IMU in a GPS/Magnetometer-aided INS

The observability of a strapdown IMU in a GPS/Magnetometer-aided INS has been investigated here when the IMU is rotated such that its angular rate with respect to the local horizontal frame $\boldsymbol{\omega}_l^{bl}$ is PWC. If the IMU does not rotate with respect to this frame, then, according to model 3 the INS error model is equal to that when the IMU is mounted on a stabilized platform. In such case, the same conditions previously obtained for full observability hold.

Assuming that the specific force $\boldsymbol{Asp}_{l,0}$ remains constant during the analysis interval, then the Lyapunov-transformed model 3 provides a PWC system if the IMU angular rate with respect to the local horizontal frame $\boldsymbol{\omega}_l^{bl}$ is PWC. However, it could not be shown whether the conditions of Theorem 1 hold, thus the simplified analysis based on the stripped observability matrix cannot be used *a priori*. On the other hand, it turns out that full observability is achieved in the first segment if some non-restrictive conditions are satisfied. Thus the analysis hereafter has verified the null space of the total observability matrix in Eq. 12.

The observability matrix for the first segment after elementary row and column operations is written in Eq. 21a. Additionally, a vector $\boldsymbol{x} \in NULL(\overline{\boldsymbol{Q}}_0')$ must satisfy the conditions in Eq. 21b.

$$\overline{\boldsymbol{Q}}_0' = \begin{bmatrix} \boldsymbol{I}_3 & \boldsymbol{0}_3 & \boldsymbol{0}_3 & \boldsymbol{0}_3 \\ \boldsymbol{0}_3 & [\boldsymbol{B}_l]_\times & \boldsymbol{0}_3 & \boldsymbol{0}_3 \\ \boldsymbol{0}_3 & \boldsymbol{0}_3 & \boldsymbol{I}_3 & \boldsymbol{0}_3 \\ \boldsymbol{0}_3 & \boldsymbol{0}_3 & \boldsymbol{0}_3 & -[\boldsymbol{B}_l]_\times \\ \boldsymbol{0}_3 & \boldsymbol{\omega}_0^*\boldsymbol{\Gamma}_0 & \boldsymbol{0}_3 & -\boldsymbol{\Gamma}_0 \\ \vdots & \vdots & \vdots & \vdots \end{bmatrix} \tag{21a}$$

$$\begin{cases} 1) & \boldsymbol{x}_1 = \boldsymbol{0}_{3\times1} \\ 2) & \boldsymbol{x}_3 = \boldsymbol{0}_{3\times1} \\ 3) & [\boldsymbol{B}_l]_\times \boldsymbol{x}_2 = \boldsymbol{0}_{3\times1} \\ 4) & [\boldsymbol{B}_l]_\times \boldsymbol{x}_4 = \boldsymbol{0}_{3\times1} \\ 5) & \boldsymbol{\omega}_0^*\boldsymbol{\Gamma}_0\boldsymbol{x}_2 - \boldsymbol{\Gamma}_0\boldsymbol{x}_4 = \boldsymbol{0}_{3\times1} \end{cases} \tag{21b}$$

Conditions 3 and 4 claim that if $\boldsymbol{x}_2$ and $\boldsymbol{x}_4$ are non-null, then they must be simultaneously aligned with $\boldsymbol{B}_l$. This condition can be mathematically represented as in Eqs. 22.

$$\begin{aligned} \boldsymbol{x}_2 &= k_0 \boldsymbol{B}_l, \quad k_0 \in \Re \\ \boldsymbol{x}_4 &= k_1 \boldsymbol{B}_l, \quad k_1 \in \Re \end{aligned} \tag{22}$$

Substituting Eqs. 22 in condition 5 leads to:

$$\boldsymbol{\omega}_0^* \boldsymbol{\Gamma}_0 (k_0 \boldsymbol{B}_l) = \boldsymbol{\Gamma}_0 (k_1 \boldsymbol{B}_l) \tag{23}$$

Assuming that the specific force $\boldsymbol{Asp}_{l,0}$ is not aligned with the IMU angular rate with respect to the local horizontal frame $\boldsymbol{\omega}_l^{bl}$, then the local geomagnetic field $\boldsymbol{B}_l$ must be aligned with the specific force $\boldsymbol{Asp}_{l,0}$ for Eq. 23 to hold, thus yielding the trivial solution to the equality. If the local geomagnetic field vector $\boldsymbol{B}_l$ is not aligned with the specific force $\boldsymbol{Asp}_{l,0}$, and since neither $\boldsymbol{B}_l$ nor $\boldsymbol{Asp}_{l,0}$ is $\boldsymbol{0}_{3\times1}$, then the only solution to conditions 3, 4, and 5 in Eq. 21b is $\boldsymbol{x}_2 = \boldsymbol{0}_{3\times1}$ and $\boldsymbol{x}_4 = \boldsymbol{0}_{3\times1}$, which claims that the system is fully observable because the null space of $\overline{\boldsymbol{Q}}_0'$ has dimension 0. This result can also be checked using Theorem A.5.

The foregoing discussion proved that the INS error model of a strapdown IMU aided by GPS and magnetometer is fully observable at the first segment if the following conditions hold:

- The specific force ($\boldsymbol{Asp}_{l,0}$) remains constant during the analysis interval;
- The IMU is rotated in such a manner that its angular rate with respect to the local horizontal frame represented in the local horizontal frame $\boldsymbol{\omega}_l^{bl}$ is PWC;
- Neither the IMU angular rate with respect to the local horizontal frame $\boldsymbol{\omega}_l^{bl}$ nor the local geomagnetic field $\boldsymbol{B}_l$ is aligned with the specific force $\boldsymbol{Asp}_{l,0}$.

One should note that these are **sufficient** conditions for full observability because only 15 lines of the observability matrix in Eq. 21a have been analyzed. The restriction regarding the alignment of the aforementioned vectors might be relaxed if more lines were added to the analysis. However, the condition should be general enough for every practical scenario. Thus, the analysis of additional lines will not be further pursued here.

Observability Analysis: Strapdown IMU in a GPS/Camera-aided INS

This scenario analysis is very similar to the one in which the IMU is mounted on a stabilized platform and thus has been omitted here. Indeed, the conclusion is the same: full observability is achieved in the first segment.

Simulations

The covariance analysis has been used to verify the observability of the INS error model. A simulated INS has been coded in Matlab. Hereafter only the scenarios regarding the novel observability analyses involving use of a calibrated magnetometer is presented due to the lack of space. The results of the observability analysis for other scenarios can be compared with previous results in the literature.

All simulations have considered ideal accelerometers and rate-gyros and thus the model noise covariance has been set to zero. The initial Kalman filter covariance and GPS and magnetometer measurement noise covariance matrices are presented, respectively, in Eqs. 24, 25, and 26 with SI units.

$$\boldsymbol{P}_0 = diag\begin{pmatrix} 10^{-6} & 10^{-6} & 10^{-6} & 10^{-4} & 10^{-4} & 10^{-4} & 10^{-6} & 10^{-6} & 10^{-6} & 10^{-10} & 10^{-10} & 10^{-10} \end{pmatrix} \tag{24}$$

$$\boldsymbol{R}_{GPS} = diag\begin{pmatrix} 10^{-10} & 10^{-10} & 10^{-10} \end{pmatrix} \tag{25}$$

$$\boldsymbol{R}_{MAG} = diag\begin{pmatrix} 10^{-20} & 10^{-20} & 10^{-20} \end{pmatrix} \tag{26}$$

where $diag(.)$ denotes a diagonal matrix.

For the sake of simplicity, the local geomagnetic field vector has been assumed to point towards north with 230.60 mGauss of intensity, which is the geomagnetic field intensity at the city of São José dos Campos, Brazil.

The first and second scenarios simulate an IMU mounted on a locally horizontal-stabilized platform in a GPS/Magnetometer-aided INS when the vehicle is subjected, respectively, to trajectories 1 and 2 in Table in which each segment lasts for 20 s. The standard deviations of the state estimation error are presented component-wise in fig. 1 for the first scenario and in fig. 2 for the second scenario. One can note that the theoretical results have been confirmed by the covariance analysis. In the first trajectory, figure 1 shows the effect of the specific force difference from segment 1 to segment 2 not in alignment with the local geomagnetic field vector. The foregoing analysis has shown that the system is then fully observable at the onset of the second segment and fig. 1 can confirm it, because the standard deviations are invariant to the specific force changes at the onset of segments 3 and 4. On the other hand, in the second trajectory seen in fig. 2, the specific force difference from segment 1 to segment 2 is aligned with the local geomagnetic field vector. Thus the system becomes fully observable only at the onset of segment 3, which is confirmed in fig. 2 since a set of standard deviations decays only after the beginning of segment 3.

The third scenario simulates a position-stationary strapdown IMU aided by GPS and a magnetometer. The IMU has been subjected to a constant angular rate with respect to the local horizontal frame about the east axis. The standard deviations of the state estimation error are presented component-wise in fig. 3. The results of the observability analysis have been verified again, since all standard deviations decay due to the IMU rotation.

Table 1. Trajectories for the first and second scenarios

Specific Force	**Trajectory 1 (m/s²)**				**Trajectory 2 (m/s²)**			
Segments	**1**	**2**	**3**	**4**	**1**	**2**	**3**	**4**
Asp_N	0	0	0.5	0	0	0.5	0.5	0
Asp_E	0	0.5	0	0.5	0	0	0	0.5
Asp_D	-g	-g	0.5-g	0.5-g	-g	-g	0.5-g	0.5-g

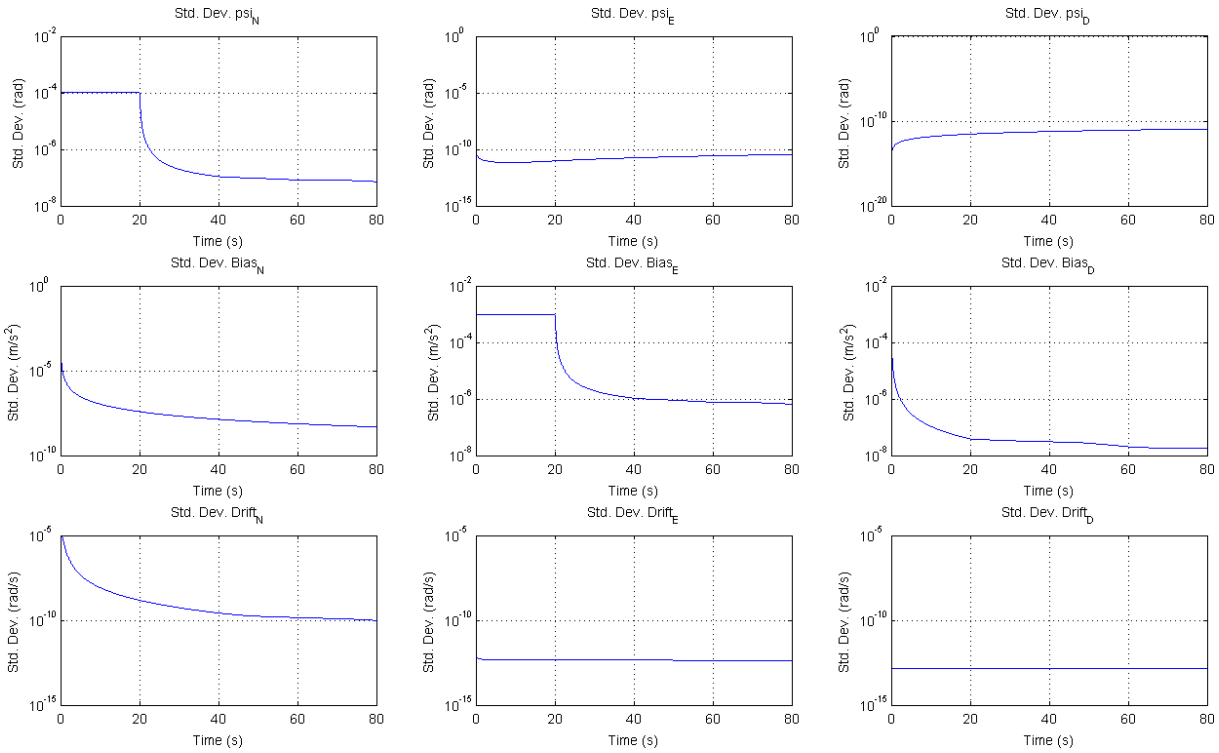

Fig. 1. Simulation results for the first scenario

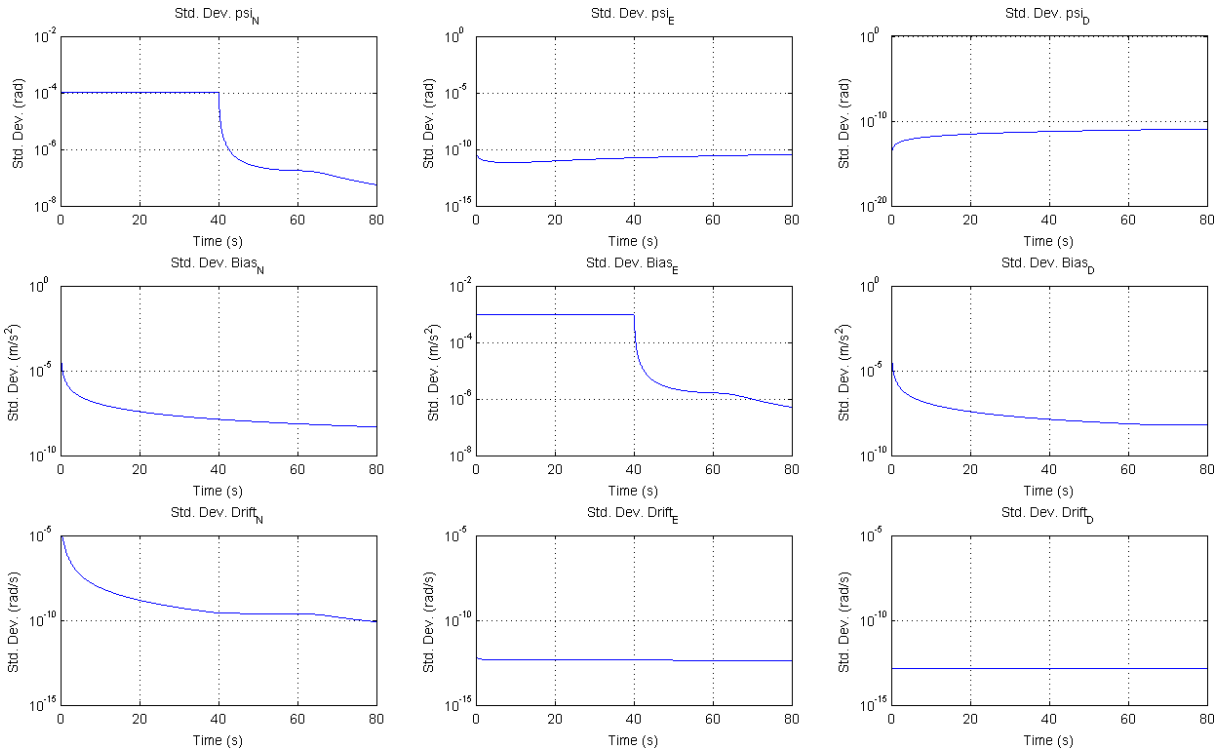

Fig. 2. Simulation results for the second scenario

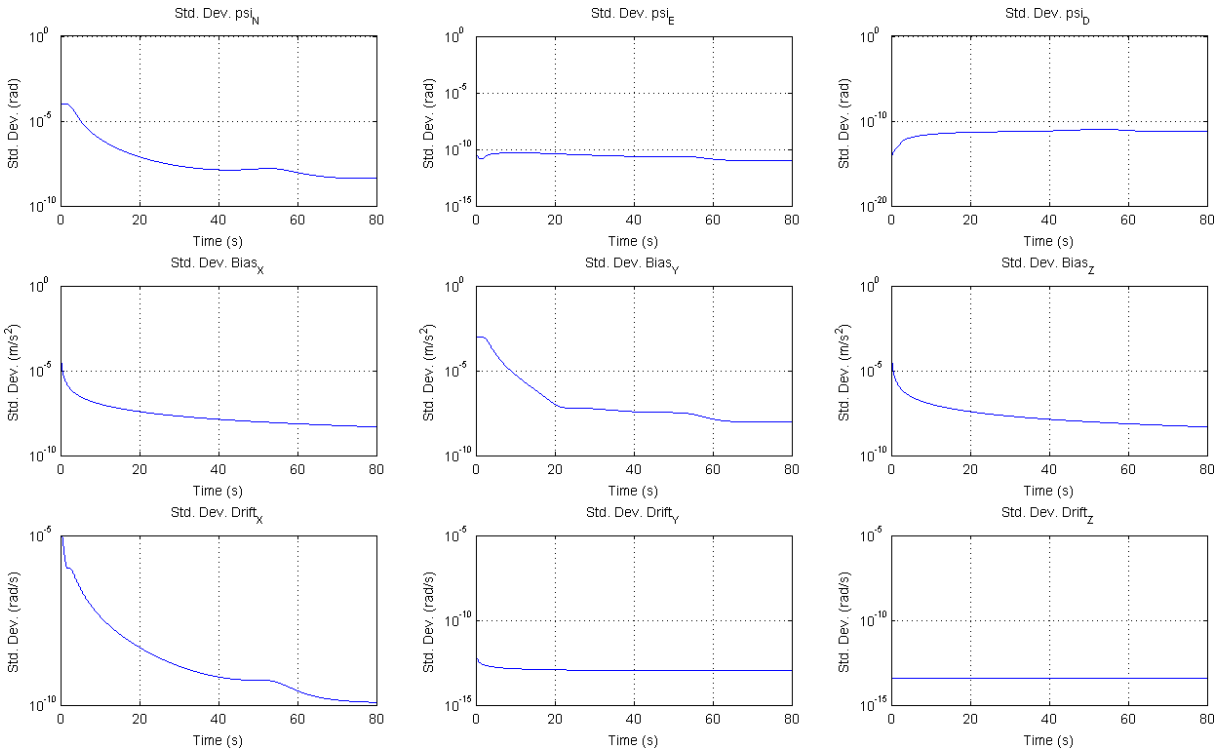

Fig. 3. Simulation results for the third scenario

Conclusions

The observability of a linear INS error model has been analyzed with distinct aiding sensors that involve both the use of GPS observables only, and usage of GPS combined with either a calibrated magnetometer or a camera when the vehicle trajectory yields piece-wise constant error dynamics. The analysis dealt with both a gyro-stabilized platform undergoing piece-wise constant specific force segments and a strapdown IMU that is also

subjected to piece-wise rotation segments. Original geometric insights related to specific forces, angular rates, the geomagnetic field, and image measurements have been derived by extending previous observability results and considering fusion with a calibrated magnetometer or a camera for INS aiding. Novel observability results were obtained in the case of aiding the INS with magnetometer and GPS. These results have been verified via simulation of the covariance of the estimation error.

Appendices

Theorem A.1: Let $\boldsymbol{x} \in \Re^3 \neq \boldsymbol{0}_{3\times1}$ and $\boldsymbol{y} \in \Re^3 \neq \boldsymbol{0}_{3\times1}$. If $[\boldsymbol{x}]_\times \boldsymbol{y} = \boldsymbol{0}_{3\times1}$, then $\boldsymbol{x}$ and $\boldsymbol{y}$ must be aligned.

Proof: The proof is trivial considering that $[\boldsymbol{x}]_\times \boldsymbol{y} = \boldsymbol{x} \times \boldsymbol{y}$.

Theorem A.2: Let $\boldsymbol{x} \in \Re^3 \neq \boldsymbol{0}_{3\times1}$ and $\boldsymbol{y} \in \Re^3 \neq \boldsymbol{0}_{3\times1}$. Thus $NULL([\boldsymbol{y}]_\times \cdot [\boldsymbol{x}]_\times^n) = NULL([\boldsymbol{x}]_\times)$, $n \in [1,2,3,4,\cdots]$, iff $\boldsymbol{x}$ and $\boldsymbol{y}$ are not orthogonal.

Proof: Left to the reader due to lack of space.

Theorem A.3: Let $\boldsymbol{x} \in \Re^3 \neq \boldsymbol{0}_{3\times1}$ and $\boldsymbol{y} \in \Re^3 \neq \boldsymbol{0}_{3\times1}$ be two orthogonal vectors, then the set of vectors $[\boldsymbol{x}, \boldsymbol{y} \times \boldsymbol{x}]$ spans $NULL([\boldsymbol{y}]_\times \cdot [\boldsymbol{x}]_\times)$.

Proof: Left to the reader due to lack of space.

Theorem A.4: Let $\boldsymbol{x} \in \Re^3 \neq \boldsymbol{0}_{3\times1}$ and $\boldsymbol{y} \in \Re^3 \neq \boldsymbol{0}_{3\times1}$ be two non-collinear vectors. If $[\boldsymbol{y}]_\times \cdot [\boldsymbol{x}]_\times^n \cdot \boldsymbol{v} = \boldsymbol{0}_{3\times1}$ holds for all $n \in [0,1,2,\cdots,L]$, $L \geq 1$, then $\boldsymbol{v} = \boldsymbol{0}_{3\times1}$ is the only possible solution.

Proof: The proof is trivial considering Theorems A.1, A.2, and A.3.

Theorem A.5: Let $\boldsymbol{x} \in \Re^3 \neq \boldsymbol{0}_{3\times1}$ and $\boldsymbol{y} \in \Re^3 \neq \boldsymbol{0}_{3\times1}$ be two non-collinear vectors. If $\boldsymbol{v} \in \Re^3$ and $\boldsymbol{w} \in \Re^3$ satisfy:

$$[\boldsymbol{y}]_\times [\boldsymbol{x}]_\times \boldsymbol{v} = [\boldsymbol{x}]_\times \boldsymbol{w},$$

then the following must hold:

$$\begin{aligned} \boldsymbol{v} &= k_0 \boldsymbol{x} + k_1 \boldsymbol{y}, & k_0, k_1 &\in \Re \\ \boldsymbol{w} &= k_2 \boldsymbol{x} + k_3 (\boldsymbol{x} \times \boldsymbol{y}), & k_2, k_3 &\in \Re \end{aligned}.$$

Proof: Left to the reader due to lack of space.

Theorem A.6: Let $\boldsymbol{x} \in \Re^3$ and $\boldsymbol{D}_a^b$ and $\boldsymbol{D}_a^c$ be the DCMs from the *a* coordinate frame to, respectively, the *b* and *c* coordinate frames. If $(\boldsymbol{D}_a^b - \boldsymbol{D}_a^c)\boldsymbol{x} = \boldsymbol{0}_{3\times1}$ holds, then $\boldsymbol{x}$ lies in the Euler axis in which a single rotation aligns the *b* coordinate frame to the *c* coordinate frame.

Proof: The condition can be rewritten as $\boldsymbol{x} = \boldsymbol{D}_b^a \boldsymbol{D}_a^c \boldsymbol{x} = \boldsymbol{D}_b^c \boldsymbol{x}$. Thus $\boldsymbol{x}$ is a vector that has the same representation in the *b* and *c* coordinate frames, then $\boldsymbol{x}$ must lie in the Euler axis in which a single rotation rotates the *b* coordinate frame into alignment with the *c* coordinate frame.

References

1. **Bar-Itzhack, I. Y.; Berman, N.** (1988). Control theoretic approach to inertial navigation systems. Journal of Guidance, Control, and Dynamics, v. 11, p. 237 – 247.
2. **Brammer, K.; Siffling, G** (1989). Kalman-Bucy Filters. Artech House Publishers, United States of America.
3. **Goshen-Meskin, D.; Bar-Itzhack, I. Y.** (1992). Observability analysis of piece-wise constant systems: Part I, Theory. IEEE Transactions on Aerospace and Electronic Systems, v. 28, n. 4, p. 1056 – 1067.
4. **Goshen-Meskin, D.; Bar-Itzhack, I. Y.** (1992). Observability analysis of piece-wise constant systems: Part II, Application to inertial navigation in-flight alignment. IEEE Transactions on Aerospace and Electronic Systems, v. 28, n. 4, p. 1068 – 1075.
5. **Lee, J. G.; Park, C. G.; Park, H. W.** (1993). Multiposition alignment of strapdown inertial navigation system. IEEE Transactions on Aerospace and Electronic Systems, v. 29, n. 4, p. 1323 – 1328.
6. **Chung, D.; Park, C. G.; Lee, J. G.** (1995). Observability analysis of strapdown inertial navigation system using Lyapunov transformation. In proceedings of the 35th IEEE Conference on Decision and Control. Kobe, Japan, p. 23 – 28.
7. **Rhee, I.; Abdel-Hafez, M. F.; Speyer, J. L.** (2004). Observability of an integrated GPS/INS during maneuvers. IEEE Transactions on Aerospace and Electronic Systems, v. 40, n. 2, p. 526 – 535.
8. **Hong, S.; Lee, H. C. M. H.; Kwon, S.; Speyer, J. L.** (2005). Observability of error states in GPS/INS integration. IEEE Transactions on Vehicular Technology, v. 54, n. 2, p. 731 – 743.

9. **Lee, M. K.; Hong, S.; Lee, M. H.; Kwon, S.; Chun, H.** (2005). Observability analysis of alignment error in GPS/INS. Journal of Mechanical Science and Technology, v. 19, n. 6, p. 1253 – 1267.
10. **Tang, Y.; Wu, Y.; Wu, M.; Wu, W.; Hu, X.; Shen, L** .(2009). INS/GPS integration: Global observability analysis. IEEE Transactions on Vehicular Technology, v. 58, n. 3, p. 1129 – 1142.
11. **Salychev, O.** (2004). Applied Inertial Navigation: Problems and Solutions. Moscow, Russia: BMSTU Press.
12. **Pinson, J. C** (1963). Inertial guidance for cruise vehicles. In LEONDES, C. T (Ed.). Guidance and Control of Aerospace Vehicles. New York, United States of America, McGraw-Hill.
13. **Chen, C.-T.** (1984). Linear system theory and design. New York, United States of America, CBS College Publishing.
14. **Bar-Itzhack, I. Y.** (1978). Optimal Updating of INS Using Sighting Devices. Journal of Guidance, Control, and Dynamics, v. 1, n. 5, p. 305 – 312.
15. **Chagas, R. A. J.** Estimação distribuída de erros em sistemas de navegação inercial auxiliada. Instituto Tecnológico de Aeronáutica, São José dos Campos, Brazil (*soon to be defended as a Ph.D. thesis, in Portuguese*).